



Green Synthesis of Biogenic Zinc Oxide Nanoflower as Dual Agent for Photodegradation of an Organic Dye and Tyrosinase Inhibitor

Anthony C. Ekennia¹ · Dickson N. Uduagwu¹ · Njemuwa N. Nwaji¹ · Obinna O. Oje¹ · Chimerem O. Emma-Uba¹ · Sandra I. Mgbii¹ · Olawale J. Olowo¹ · Obianuju L. Nwanji¹

Received: 8 July 2020 / Accepted: 26 August 2020 / Published online: 5 September 2020
© Springer Science+Business Media, LLC, part of Springer Nature 2020

Abstract

In the study, metabolites of *Euphorbia sanguinea* were used as benign reducing and stabilizing agents to obtain zinc oxide nanoparticles (ZnO-NPs). The nanoparticles were evaluated as dual agent for photodegradation of Malachite green dye and *tyrosinase* inhibitor of mushroom tyrosine enzyme. Surface plasmon bands and energy band gaps of the ZnO-NPs were within the range 356–378 nm and 2.72–4.37 eV respectively as obtained from the UV–Vis spectra. SEM/EDS elemental mapping of the nanoparticles gave flower-like shape and even distribution of zinc and oxygen. XRD result revealed crystallographic peaks assigned to hexagonal phase of zinc oxide. The metal oxide nanoparticles were used to achieve 53% percentage degradation of Malachite green dye solution in less than a minute of solar radiation, which increased to 92% in 60 min. A first order kinetics with correlation coefficient R^2 of 0.937, rate constant of 0.0084 min^{-1} and half-life of 82.52 min was established for the photodegradation process. The ZnONPs exhibited good *tyrosinase* inhibition with IC₅₀ of 49.016 $\mu\text{g/ml}$. The mode of enzymatic inhibition was competitive with an inhibition constant (K_i) of 0.525 mM using Lineweaver–Burk kinetic model.

Keywords Zinc oxide · Nanoparticles · Photocatalytic · Tyrosinase inhibition · Kinetics

1 Introduction

In recent times, nano-biotechnology has become the focal point of many scientific explorations because it is in tandem with the principles of green chemistry [1]. Diverse plant metabolites have been explored for biosynthesis of various metal(oxide) nanoparticles [2, 3]. Biosynthesized nanoparticles are mostly non-lethal and possess important physicochemical properties such as: large specific surface area, controlled surface activity, high surface interface, catalytic, optical and volume effects. Hence, they have been applied in water treatment, photocatalytic degradation of dyes, cosmetics and medicine [4]. Remarkably, the rich heritage of plant diversity offers great potential for bio-prospecting in nanotechnology [4], biotechnology [5], Science [6, 7] and engineering [8, 9].

Organic dye pollutants pose a challenge to the environment due to their toxicity, non-biodegradability, kinetically slow degradation process and carcinogenicity [10–12]. Several techniques such as: adsorption, ion exchange, coagulation–flocculation, membrane technology, direct chemical oxidation, irradiation and advanced oxidation processes have been employed in the treatment of wastewater containing dye molecules. However, advanced oxidation processes (AOP) has gained more attention compared to other techniques because it is cost effective, has good chemical oxygen demand (COD) value and very efficient in the removal of residual dye colouration from wastewater [13]. Photocatalytic degradation of organic dye pollutants using metal oxide nanoparticles is a form of AOP that employs interaction between dye molecules in wastewater and radicals generated by the metal nanoparticles when photon energy is absorbed on illumination from the sun or a UV–Vis source [14]. Photocatalytic degradation of organic dye pollutants using plant mediated ZnO nanoparticles has been extensively reported [15, 16]. However, there are no reports on the photocatalytic degradation of organic dyes using ZnO nanoparticles obtained from aqueous leaf extract of *Euphorbia Sanguinea*.

✉ Anthony C. Ekennia
chemisttony@gmail.com

¹ Department of Chemistry/Biochemistry and Molecular Biology, Alex Ekwueme Federal University, Ndufu-Alike (AE-FUNAI), P.M.B 1010, Abakaliki, Ebonyi State, Nigeria

In addition, kinetic study of photocatalytic degradation of organic dyes and their mechanisms of action under illumination by sunlight are scarce.

Tyrosine enzyme is utilized by plants in the production of phenolic polymers like tannins, lignin, flavonoids and for the regulation of redox potential during plant cell respiration and healing of wounds in plants [17]. It is also involved in the conversion of monophenols to diphenols by monophenolase activity and further conversion of diphenols into quinones by diphenolase activity. Over expression of tyrosinase in plants has been implicated in enzymatic browning of fruits and vegetables, leading to loss of their nutritional values. This has posed a huge challenge in food availability and storage [18]. However, the use of biosynthesized metal nanoparticles in tackling this challenge is scarce and not reported in details.

Euphorbia sanguinea is a plant mostly found in the tropical and subtropical regions of Africa. It is of the genus *Euphorbia*, from the spurge family, Euphorbiaceae. Some species of the genus have been reported to be used locally for the treatment of skin diseases, migraine, and intestinal parasites [19]. Methanolic extracts of the stem sap of *Euphorbia sanguinea* was reported to contain flavonoids and saponins [20]. However, the biochemical components of aqueous leaf extract of the plant is yet to be reported. Also, metabolites of the leaf extract have not been explored in the synthesis of metal oxide nanoparticles to the best of our knowledge. Hence, in the present study, we report the evaluation of the phytochemical properties of the aqueous extract of *Euphorbia sanguinea*. The plant extracts were explored in the synthesis of zinc oxide nanoparticles. The nanoparticles were evaluated for their tyrosinase inhibition activity using mushroom tyrosine bioassay and their photocatalytic degradation of Malachite green dye. The kinetics and mechanisms of action of the two experiments were also discussed in details.

2 Experimental Section

2.1 Materials

Zinc chloride, sodium hydroxide, malachite green dye, ascorbic acid, sodium phosphate dibasic heptahydrate, sodium phosphate monobasic monohydrate, tyrosine enzyme (from mushroom, 25KU) and 3,4-dihydroxyphenylalanine (L-DOPA) were obtained from Sigma (USA). *Euphorbia sanguinea* leaves were obtained from Calabar, Nigeria.

2.1.1 Apparatus and Instrumentation

Microscopic Characterization The surface morphology, elemental composition and size of the AgNPs were analyzed using scanning electron microscope (SEM) FEIXL 30, equipped with Energy Dispersive X-ray (EDS). X-ray

diffraction (XRD) patterns were measured on a Bruker s D8 Discover diffractometer, equipped with a Lynx Eyedetector, under Cu-K α radiation ($\lambda = 1.5405 \text{ \AA}$). Data were collected in the range from $2\theta = 10$ to 90 , scanning at 0.0101 min^{-1} and 192 s per step. The samples were placed on a zero-background silicon wafer slide. Optical characterization: the Ultraviolet–visible spectra were analyzed with Agilent Technologies Cary 60 spectrophotometer and the Fourier transform-infrared (FTIR) spectra were recorded on Agilent Technologies spectrophotometer.

2.2 Aqueous Extraction of the *E. sanguinea* Leaf

Euphorbia sanguinea leaves were freshly collected washed thrice with deionised water and left to air-dry at room temperature. The dried leaves were ground into fine particles using a ceramic pestle and mortar. 4 g of the finely-divided leaf particles was dissolved in 200 ml of deionized water. It was heated in a water bath at $80 \text{ }^\circ\text{C}$ for 45 min. The aqueous leaf extract was filtered using a Whatmann filter paper, put into an amber bottle and stored in the refrigerator.

2.3 Phytochemical Characterization of the Aqueous Leaf Extract of *E. sanguinea*

Qualitative and quantitative characterisations of the aqueous leaf extract of *E. sanguinea* were carried out using standard procedures as reported in literature [21, 22].

2.4 Phytosynthesis of Zinc Oxide Nanoparticles

Zinc oxide nanoparticles were synthesized according to methods reported in literature with little modifications [23, 24]. 1.34 g (0.1 M) of ZnCl_2 was weighed and dissolved with 98 ml of deionized water. The mixture was poured into a flat bottom flask and heated on a magnetic stirrer at $90 \text{ }^\circ\text{C}$. 2 ml of the plant extract was added in drops to the stirred salt solution. The pH of the mixture was altered to basic using 2 M NaOH solution. The mixture was stirred for 2 h after which it was filtered under gravity and the residue was dried at $60 \text{ }^\circ\text{C}$ in the oven for 48 h. The same procedure was also carried out using 1 ml, 1.5 ml and 3.5 ml of the plant extract added to the same concentration of zinc chloride salt.

2.5 Tyrosine Inhibition Activity

Tyrosinase inhibitory activity of the nanoparticles was carried out using spectrophotometric method [25]. Briefly, 50 $\mu\text{g/ml}$ of ZnO nanoparticles was added to 3.0 ml of a reaction mixture containing 0.1 mM of L-DOPA, 0.1 mM of sodium phosphate buffer (pH 6.5) and 50 U/ml of mushroom tyrosinase. The mixture was incubated at room temperature for 30 min. The formation of dopachrome was monitored

at 475 nm with an UV–Visible spectrophotometer (Double beam, Curry C60). The percentage of the inhibition of tyrosinase activity was calculated using Eq. (1):

$$\text{Tyrosinase inhibitory activity (\%)} = A - \frac{B}{A} \times \frac{100}{1} \quad (1)$$

where A is absorbance of blank solution after incubation, B is absorbance of sample solution after incubation.

The experiment was repeated for other concentrations (500 µg/ml, 300 µg/ml, 200 µg/ml and 100 µg/ml) of ZnONPs. The effect of the substrate was monitored in the presence and absence of the ZnO nanoparticles with different concentrations (0.5, 0.75, 1.25 and 1.5 mM) of L-DOPA. The mode of inhibition and inhibition parameters: Lineweaver–Burk constant (K_m), maximum velocity (V_{max}) and the inhibition constants were established using Lineweaver–Burk plots.

2.6 Photocatalytic Degradation of Malachite Green Dye

The photocatalytic degradation experiment was done according to methods in literature [26, 27]. 8 mg of the ZnO nanoparticles was added to 1.5 mg/l of Malachite green dye solution. The solution was stirred vigorously to ensure equilibration and incubated in the dark for 30 min. The reaction mixture was exposed to illumination from sunlight and monitored using a UV–Vis spectrophotometer at different time intervals (0, 5, 15, 30, 45, 60 min). The percentage degradation was obtained using Eq. (2):

$$\text{Percentage degradation (\%)} = C - \frac{S}{C} \times \frac{100}{1} \quad (2)$$

where C is absorbance of blank solution (dye solution) after incubation, S is absorbance of sample solution (dye and nanoparticles) after incubation.

3 Results and Discussion

3.1 Phytochemical Analysis

Results of qualitative and quantitative analysis of aqueous extract of *E. Sanguine* leaves are presented in Tables 1 and 2 respectively. Qualitative analysis in Table 1 showed the presence of polyphenols, steroids, terpenoids, alkaloids, flavonoids, tannins, reducing sugars, carbohydrates and glycosides.

Results of the quantitative analysis in Table 2 showed high amount of total phenolics, carbohydrate, flavonoid, alkaloids and reducing sugars. These plant metabolites have been described as reducing and stabilizing agents in

Table 1 Results of phytochemical analysis of aqueous leaf extract of *E. sanguinea*

Phytochemicals	Availability
Reducing sugars	++
Alkaloids	++
Flavonoid	++
Tannin	++
Total phenolics	+++
Steroids	+++
Terpenoids	+++
Saponins	–
Carbohydrate	++
Glycosides	+

(+) present; (–) absent

Table 2 Quantitative phytochemical results of the plant extract

S.N	Phytochemicals	Quantity (STD) (ml/100 g)
1	Glycosides	0.166 ± 0.004
2	Reducing sugars	107.59 ± 1.199
3	Alkaloids	197.025 ± 2.466
4	Flavonoid	160.389 ± 1.802
5	Tannin	4.396 ± 0.083
6	Total Phenolics	2691.410 ± 27.822
7	Terpenoids	19.793 ± 0.790
8	Saponin	–
9	Carbohydrate	467.075 (± 4.925)

Result expressed as Mean ± standard deviation (SD)
n = 3

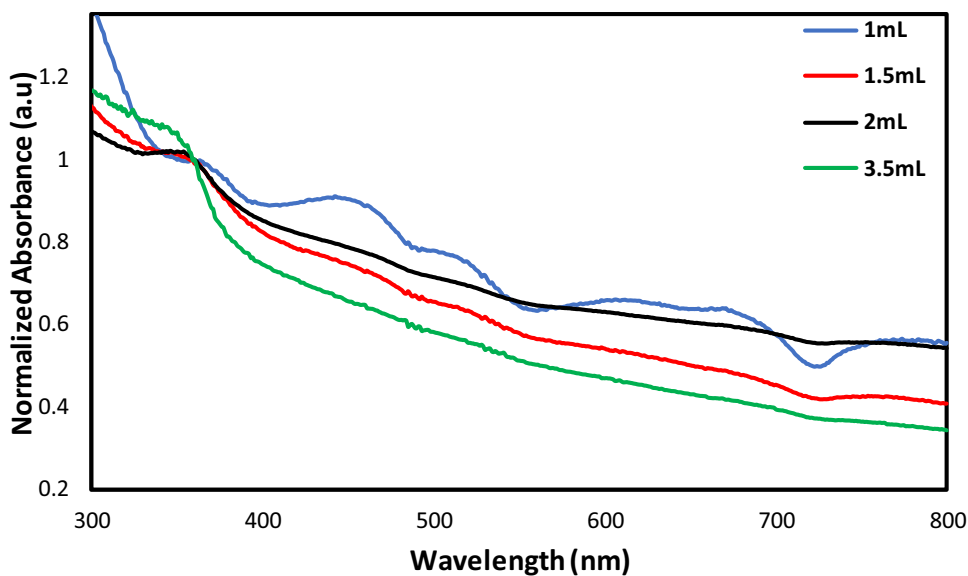
biosynthesis of metal nanoparticles and have also been used as antioxidants and tyrosinase inhibitors [5, 28].

3.2 UV–Vis Spectral Analysis

The normalized absorption spectra of the various ZnO nanoparticles obtained by varying the concentration of the plant extract (1–3.5 ml) are shown in Fig. 1.

The intense surface plasmon absorption bands for all samples were observed between 350 and 400 nm corresponding the excitonic absorption of the ZnO-NPs and were found to be within the same range of surface Plasmon bands for ZnO nanoparticles obtained from plant extracts of *Turbinariaconoides* (360 nm), *Parthenium hysterophorus* (400 nm) and *Catharanthus roseus* (350 and 500 nm) [28–30]. The surface plasmon bands becomes more pronounced with the increase in concentration of the extract which could be attributed to enhancement in reduction properties with concomitant increase in nucleation and size of the nanocrystals arising from deficiency of oxygen, surface defects, impurity centres and difference in band gap [14].

Fig. 1 UV–Vis spectra showing the surface plasmon bands of ZnO nanoparticles with variation in volume of plant extracts precursor from 1 to 3.5 ml



Band gap of a semiconductor is the distance between the valence band and the lowest empty conduction band. It is a determinant of the amount of photon energy needed to be absorbed by the semiconductor to cause photo-generation of photoelectron and holes. The results of the absorption spectra were used to determine the band gap energy of each of the ZnO nanoparticles (Fig. 2) using Tauc’s equation in (Eq. 3) for direct band gap material [14]:

$$(\alpha h\nu)^2 = k(h\nu - E_g) \tag{3}$$

where $h\nu$ is the photon energy, E_g is the band gap energy, k is a constant and α is absorption constant.

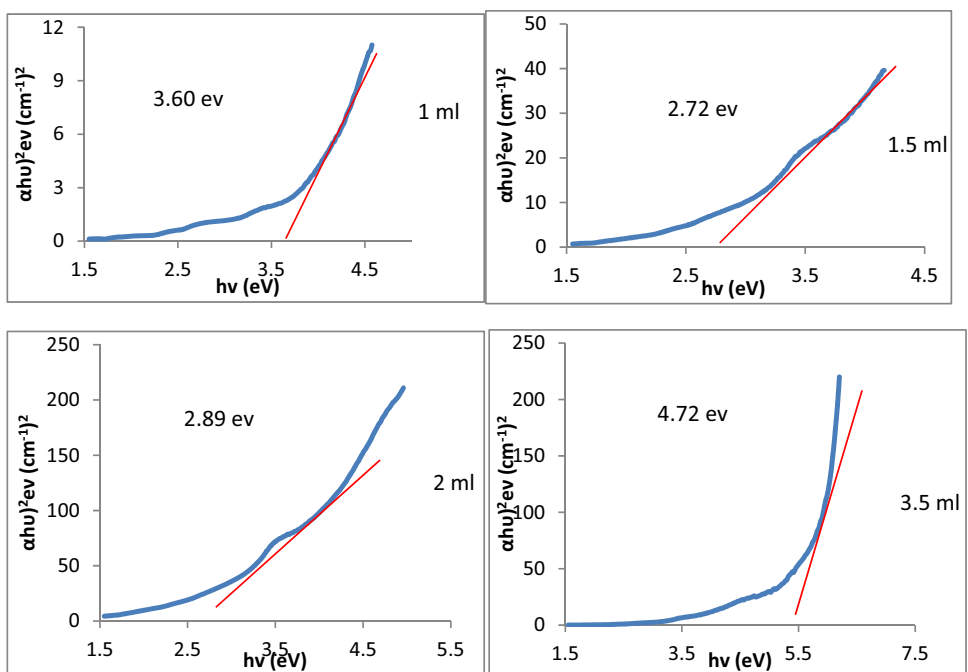
Equation 3 can be further expressed as:

$$(2.303 * A * 1240/\lambda)^2 = k(1240/\lambda - E_g) \tag{4}$$

where A and λ are absorbance and wavelength respectively obtained from the absorption spectra of the nanoparticles. A plot of Eq. 4 gives an absorption curve whose tangent expresses the energy band gap of the nanoparticles.

Biosynthesized ZnO nanoparticles have been reported to show band gap energy of 2.88 eV and 3.10 eV [31]

Fig. 2 Tauc’s plots for the energy band gap of the ZnO nanoparticles



3.28 eV [32] and 3.31 eV [33]. From the results in Fig. 2, the band gap energy for the ZnO nanoparticles are within the reported range. However, the ZnO nanoparticles obtained using 1 ml of the plant extract precursor gave the closest band gap energy to 3.37 eV, which is the theoretical value for an undoped ZnO nanoparticle.

3.3 FT-IR Spectral Analysis

The plant extract and a representative sample of the ZnO nanoparticles (ZnO-NPs@1 ml) were subjected to FT-IR analysis at room temperature to evaluate the functional groups of the plant metabolites that participated in the reduction and stabilization of the nanoparticles. The FT-IR spectra of the compounds are shown in Fig. 3a and b.

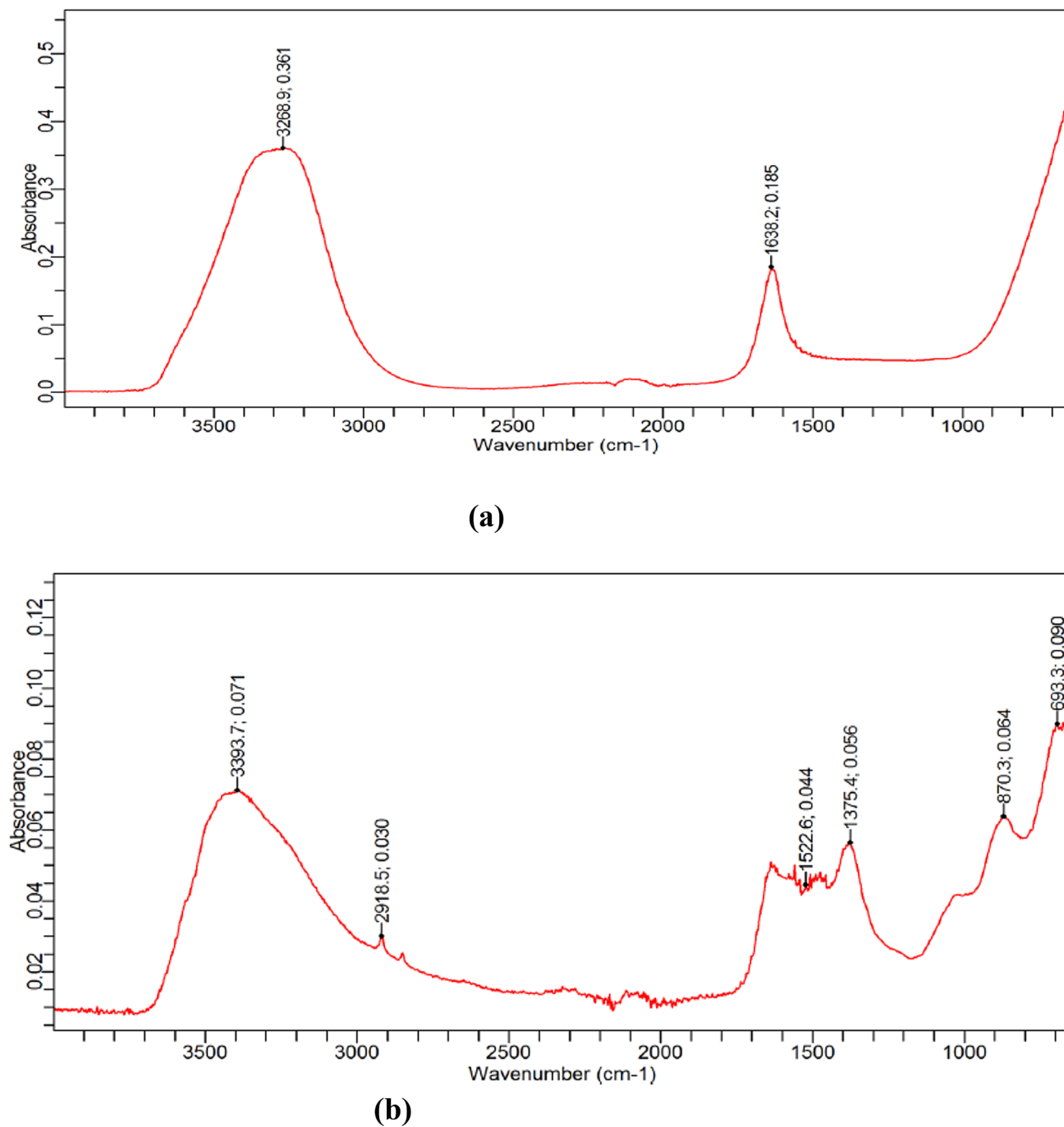


Fig. 3 FT-IR spectra for **a** plant extract and **b** ZnO nanoparticles (ZnO-NPs@1 ml)

The significant functional groups of the plant extracts gave vibrational bands as shown in Fig. 3a. The OH stretching band which could be from polyphenols, flavonoids, reducing sugars, alkaloids and tannins was seen as a broad at 3269 cm^{-1} . The band was seen at a higher wave number of 3394 cm^{-1} in the spectrum of the ZnO-NPs due to the participation of the hydroxyl groups in stabilization of the metal oxide nanoparticles [34]. The band at 1638 cm^{-1} in Fig. 3a which was attributed to N–H bending of amines in alkaloids or C=O stretching in polyphenols, flavonoids, and reducing sugars was also observed in Fig. 3b at lower wavenumbers [35]. The presence of these bands in Fig. 3b is due to their participation in the formation of the nanoparticles [36]. A metal–oxygen bond vibration was observed at 693 cm^{-1} in the spectrum of the ZnO nanoparticles which is characteristic to Zn–O vibrational stretching that further confirmed the formation of ZnO-NPs [37].

3.4 Microscopy Analysis

3.4.1 Scanning Electron Microscopy

The morphological of the synthesized nanoparticles as examined using scanning electron microscopy and presented at Fig. 4a and b showed flower-like shape [38]. A petal-like flower shape was observed when 1 ml extract was used, which gradually changed to fusiform flower shape when 2 ml extract was used. This could be attributed to increase in lattice decomposition arising from higher concentration of the extract. The average size of 34 nm was observed through random selection of 50 clustered lumps of the nanocrystals due to lack of monodispersity in shape of flower-like particles. The average thickness of the nanocrystals was found to be 5 nm and 8 nm for the 1 ml and 2 ml extract respectively.

3.5 Energy Dispersive X-ray Analysis

The energy dispersive X-ray diffractive (EDX) study was carried out for the synthesized ZnO-NPs to elucidate the

elemental composition. EDX study presented in Fig. 5 validates the presence of elemental Zn (zinc) and O (oxygen) from the peak obtained thus confirming the formation of the ZnO nanoflowers [38]. The elemental mapping showed evenly distribution of zinc and oxygen throughout the nanoflowers indicating high crystallinity with no obvious impurity.

3.6 X-ray Diffraction Analysis

The XRD pattern of the ZnO nanoflower is shown in Fig. 6. The crystallographic peaks observed at $2\theta = 32.09, 34.53, 36.33, 47.64, 57.69, 63.07$ and 68.26 correspond to (100), (002), (101), (102), (110), (103) and (112) crystallographic phase of hexagonal zinc oxide (JCPDS card no. 36-1451) [39]. The average crystalline diameter of the nanocrystals determined using the Scherrer Eq. (5) was found to be 27 nm and 33 nm, which are very close to the observed sizes using SEM [40].

$$D = \frac{k\lambda}{\beta \cos \theta} \quad (5)$$

3.7 Catalytic Degradation of Malachite Green Dye

The photocatalytic ability of the zinc oxide nanoparticles was evaluated during the degradation of malachite green (MG) dye in aqueous solution under sunlight illumination. The results of time-dependent percent degradation of malachite green (MG) was presented at Figs. 7 and 8. UV–Vis absorption spectrum (blue) of malachite green (MG) solution gave two peaks: at 434 nm and 623 nm. Photo-degradation of MG was portrayed by a decrease in blue-green colour intensity of the dye with increase in irradiation time and a reduction of the maximum absorption peak of the dye [41, 42].

Fig. 4 SEM of ZnO particles; **a** (ZnO-NPs@1 ml), **b** (ZnO-NPs@2 ml)

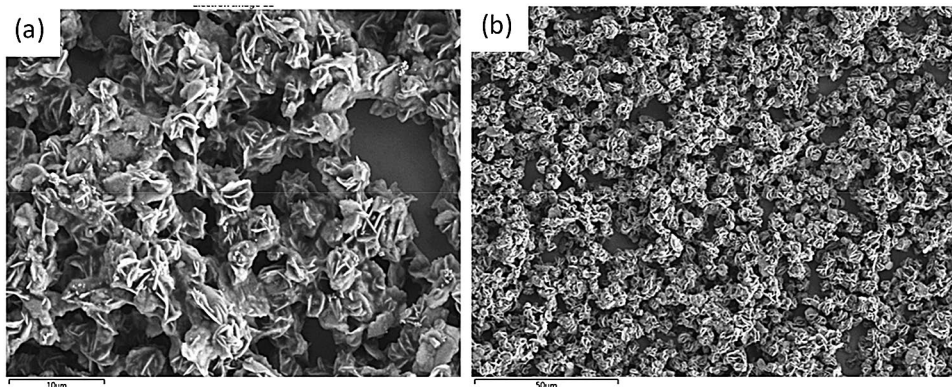


Fig. 5 EDX elemental mapping showing that Zn and O is uniformly distributed in the ZnO nanoflower

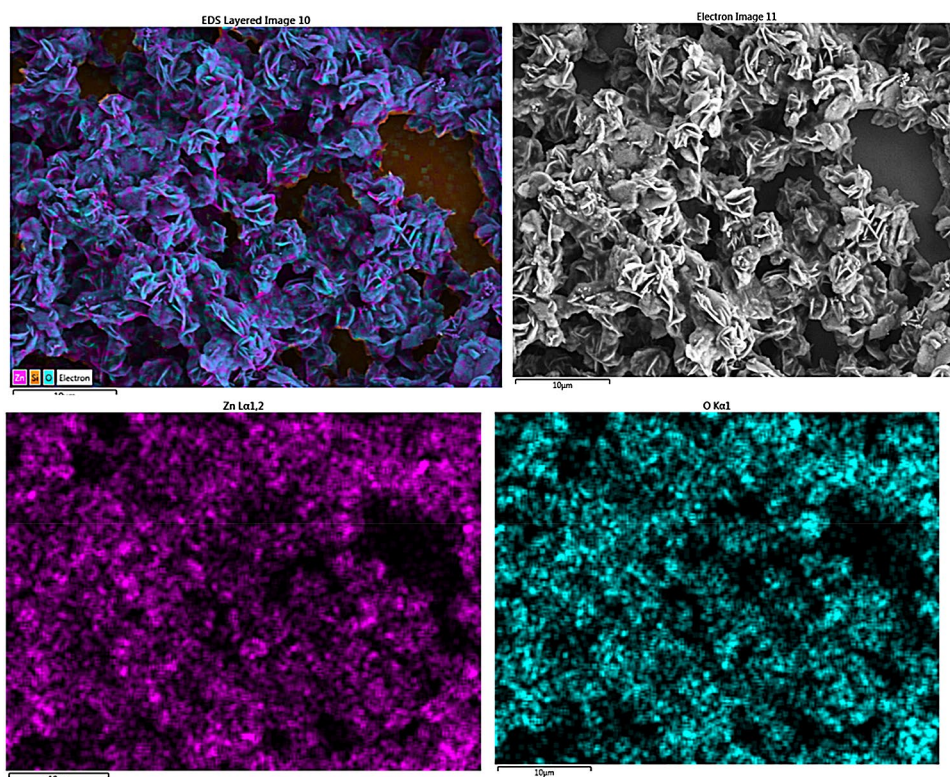
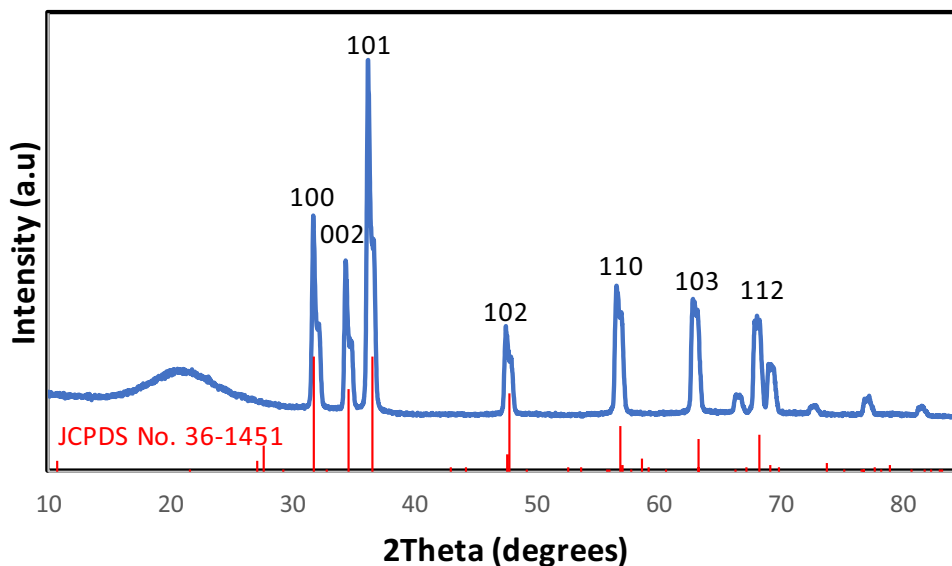


Fig. 6 XRD of the ZnO nanoparticles



As shown in Figs. 7 and 8, the concentration of MG dye decreased with respect to time of contact with the ZnO photocatalyst. It was found that in less than a min of illumination of the MG dye solution with ZnO nanoparticles, 53% degradation of the MG dye was achieved. Afterwards, there was a marked increase in percentage degradation of MG from 53 to 87% as the contact time increased from 0–5 min;

however, after 5 min, the degradation rate was gradual until 60 min when 92% degradation was achieved.

In 60 min, the degradation of MG dye solution was almost complete. The MG solution, in the absence of the ZnO NPs, did not show any degradation under solar irradiation. Thus, it was confirmed that the ZnO nanoparticles were responsible for the degradation of MG under the solar irradiation. The Photocatalytic degradation results

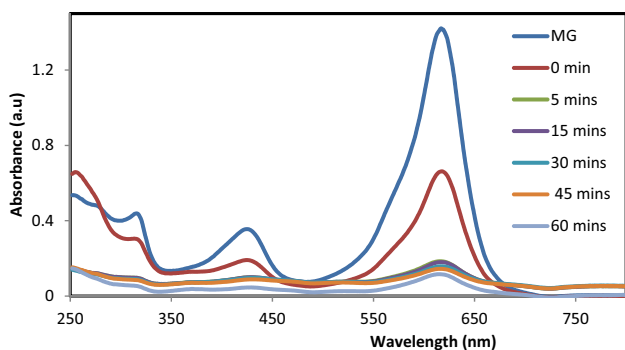


Fig. 7 UV–Vis spectra showing catalytic degradation of Malachite green by ZnO nanoparticles with variation of contact time

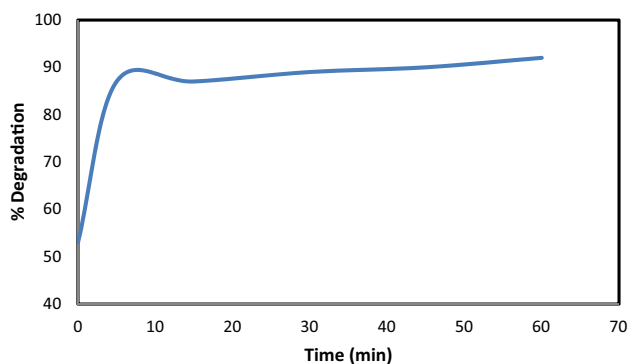
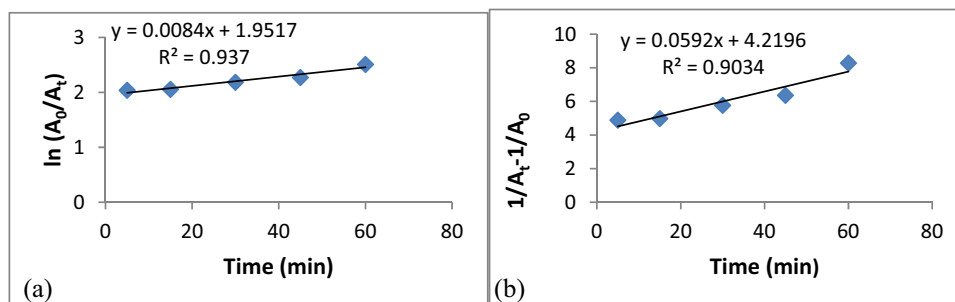


Fig. 8 Percentage degradation of MG with time

obtained are significant improvement to those reported in literature: Ma et al. reported 64% degradation of malachite green using TiO_2 nanoparticles after 1 h [43], Wang et al. recorded 68% degradation of malachite green using hybrid of ZnO nanorods grown on three-Dimensional reduced graphene oxide/Ni Foam [44] and Kaneva et al reported 89% degradation of malachite green using undoped ZnO nanoparticles [45].

Fig. 9 **a** first order kinetics for degradation of MG, **b** second order kinetics for degradation of MG



3.7.1 Kinetics of the Photocatalytic Process

The experimental result of the photocatalytic degradation of MG were further analyzed by using the pseudo first-order and pseudo second-order kinetic models. The linear equations for the pseudo first and pseudo second order kinetic models, as well as, their respective half-life equations are shown in Eqs. (6–9) respectively [46].

$$\ln \frac{A_0}{A_t} = k_1 t \quad (6)$$

$$\frac{1}{A_t} - \frac{1}{A_0} = k_2 t \quad (7)$$

$$t_{1/2} = \frac{\ln 2}{k_1} \quad (8)$$

$$t_{1/2} = \frac{1}{k_2 A_0} \quad (9)$$

where A_0 is initial absorbance; A_t is absorbance at time t ; k_1 and k_2 are rate constants for first order and second order reactions respectively; $t_{1/2}$ is half-life.

The kinetics of the degradation of process can be visualised in Fig. 9a and b for first order and second order reactions respectively. First order kinetic model gave the best fit for the photo-degradation of MG with a correlation coefficient, R^2 of 0.937 which is higher than that of pseudo-second order model with a correlation coefficient R^2 of 0.9034. A linear relationship between $-\ln(A_0/A_t)$ and reaction time (t) further indicate that the photocatalytic reaction followed the Langmuir–Hinshelwood model [41]. The rate constant and half-life for the first order reaction are 0.0084 min^{-1} and 82.52 min while those of the second order reaction are 0.0592 min^{-1} and 12.36 min respectively.

3.7.2 Mechanism of Photocatalytic Action

The photocatalytic degradation of dye molecules in water can be ascribed to be an advanced oxidation process (AOP) of dye remediation. Similar to the use of photo-Fenton method in the degradation of dye molecules in which solar radiation initiates the oxidation of Fe(II) to Fe(III) causing the formation of a radical that interacts with the dye molecule to mineralize the dye to CO₂ and H₂O [47], the photocatalytic process is initiated by placing the ZnO-NPs and dye solution in the presence of solar radiation. The photon energy from the sun is absorbed by the semiconductor ZnO-NPs causing electronic transition (or photoelectron generation) from its valance band (VB) to the lowest empty conduction band (CB). This transition creates conjugated photo hole on the surface of the ZnO-NPs. The photon electron interacts with oxygen absorbed on the surface of the photocatalyst to produce superoxide radical ($\cdot\text{O}_2^-$), while the hole reacts with H₂O in the solution to generate a hydroxyl radical ($\cdot\text{OH}$). The radicals cause series of oxidation and reduction of the organic dye molecules to their various intermediates and eventually into their respective end products of CO₂ and H₂O [48].

Photocatalytic degradation involves two main processes: adsorption–desorption and photodegradation [49]. In the first 5 min, the rate of adsorption of the dye molecules on the surface of the photocatalyst was high and hence high rate of degradation within 0–5 min of contact time (53–83%) was recorded. The interaction of the dye with the surface of the ZnO-NPs could be through hydrogen bonding of the amine group of the dye or electrostatic interaction between the positively charged surface of the photocatalyst and the anionic dye molecules. As the contact time progresses, the adsorption sites on the surface of ZnO-NPs are increasing loaded, therefore rate of adsorption will be much slower as the saturation point is reached. Hence, a decrease in the rate of degradation within 30–60 min of contact time (87–92%) was observed. On the surface of the ZnO-NPs, powerful oxidants $\cdot\text{O}_2^-$ and $\cdot\text{OH}$ cause the degradation of the dye molecules to end products (CO₂

and H₂O) and desorption occurs leading to adsorption of more molecules.

3.7.3 Stability of Photocatalyst ZnO-NPs

A good photocatalyst must be stable for large scale processes and should be able to be regenerated and reused. Hence, we investigated the stability of the ZnO-NPs by carrying out recycling experiments of the photocatalytic degradation of Malachite green dye under irradiation from sunlight. The results are presented in Table 3.

The photocatalyst was collected after each cycle by centrifugation, then washed with distilled water and ethanol and dried in an oven at 80 °C [50]. The sample was then reused for subsequent degradation. As can be seen, the removal rate of Malachite green dye decreased from 92 to 80% within 60 min of contact time after three cycles. The photocatalytic activity of ZnO only minimally decreased, due to the unavoidable loss of photocatalysts during the cycle processes.

3.8 Tyrosinase Inhibition Activity of ZnO-NPs

The antityrosinase activity of the synthesized ZnO-NPs was represented in Fig. 10. The results depicted a dose dependent activity with an IC₅₀ of 49.016 µg/ml. The metal oxide nanoparticles have higher tyrosinase inhibition activity compared to the plant extract with 36% inhibition. The standard drug, ascorbic acid gave 77% tyrosinase inhibition at 100 µg/ml.

The result obtained is an improvement to some literature reports i.e. tyrosinase inhibition activity of ZnO nanoparticles obtained from brown seaweed-*turbinariaconoides* was 38% at a concentration of 50 µg/ml [51].

3.8.1 Enzyme Kinetic Study and Mechanism of Anti-tyrosinase Action

The kinetics of the tyrosinase inhibition was studied using Lineweaver–Burk plot and presented in Fig. 10. From the

Table 3 Result of different runs of the photocatalytic degradation experiments

Name	Time (min)	1st Photocatalytic experiment (%)	2nd Photocatalytic experiment (%)	3rd Photocatalytic experiment (%)	4th Photocatalytic experiment (%)
ZnO-NPs	0	53	53	49	45
ZnO-NPs	5	87	86	82	61
ZnO-NPs	15	87	86	84	70
ZnO-NPs	30	89	89	88	72
ZnO-NPs	45	90	89	90	76
ZnO-NPs	60	92	92	90	80

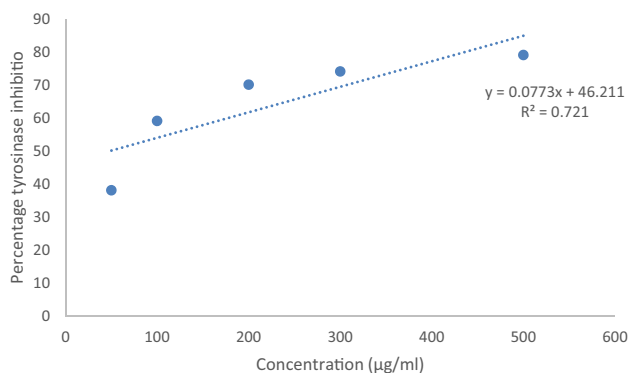


Fig. 10 Tyrosinase inhibition activity of ZnO-NPs

plot, the kinetic parameters in the absence of ZnO-NPs revealed that the maximum velocity (V_{max}) of the enzyme is 0.32 mM/min while the affinity of the enzyme for L-DOPA (K_m) is 1.071 mM. On the introduction of 50 µg/l of the ZnONPs, the V_{max} was found to be approximately 0.33 mM/min while the K_m was calculated to be 1.59 mM. The result clearly showed that the V_{max} of the reaction was not affected by the inhibitor but there was an increase in K_m (Fig. 11).

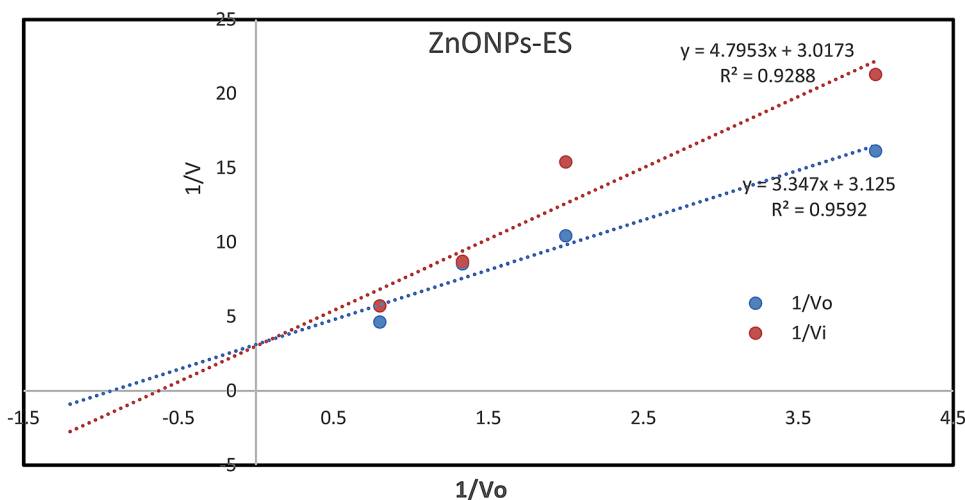
This observation is characteristic of a competitive mode of inhibition where the inhibitor and substrate compete for the active site of the enzyme [52]. In this type of inhibition, the double reciprocal plot of the two plots: catalysed and inhibited plots, normally intercept at a point on the $1/V$ axis. Hence the mechanism of tyrosinase inhibition by the

ZnO-NPs is proposed to involve the nanoparticles compete for the active site of the enzyme with the substrate thereby preventing the substrates from binding to the active site of the enzyme. The inhibition constant K_i of the ZnO-NPs which shows the affinity of binding of the inhibitor and the enzyme was calculated as 0.525 mM. The initial velocity (V_o) of the enzyme was calculated at the substrate concentration of 0.1 mM to be 0.027 mM/min while in the presence of the ZnO-NPs (inhibitor) the initial velocity was calculate to be 0.0003 mM/min, thereby giving a relative activity of 0.011 and a percentage fractional inhibition of 98.8% showing very high inhibitory effect on the enzyme [53].

4 Conclusion

We presented zinc oxide nanoflowers that were obtained using a low cost and green method involving aqueous leaf extract of *E. sanguinea*. The nanoflowers were used as photocatalysts in the degradation of Malachite green dye and also as *tyrosinase* inhibitor for mushroom tyrosine enzyme. The formation of the ZnO-NPs was confirmed by results obtained from UV–Vis spectra, SEM, EDX and XRD. The zinc oxide nanoflowers gave good photocatalytic efficiency in the degradation of the Malachite green dye solution with 53% percentage degradation in less than a minute of solar radiation which improved to 92% in 60 min of exposure. In addition, ZnO-NPs exhibited competitive type of tyrosinase inhibition with IC_{50} of 49.016 µg/ml.

Fig. 11 UV-Vis spectra of ZnO nanocrystals with different concentration of extract



Acknowledgements The authors are grateful to Alex Ekwueme Federal University Ndufu-Alike, Nigeria for the provision of laboratory space and research equipment.

Author Contributions The research idea was conceptualized by ACE and DNU; all authors participated in synthesis, applications and manuscript preparations.

Compliance with Ethical Standards

Conflict of interest The authors declare that they have no known competing financial interests or personal relationships that could have appeared to influence the work reported in this paper.

References

- V.K. Vidhu, P. Daizy, *Micron* **56**, 54–62 (2014)
- M.C. Mahesh, E.N. Shivayogeeswar, K.R. Kotresh, *SN Appl. Sci.* **1**, 117 (2019). <https://doi.org/10.1007/s42452-018-0095-7>
- J. Huang, L. Lin, D. Sun, H. Chen, D. Yang, Q. Li, *Chem. Soc. Rev.* **44**(17), 6330–6374 (2015)
- B. Nagaraj, I. Akber, R.L. Yong, *Mater. Lett.* **129**, 28–30 (2014). <https://doi.org/10.1016/j.matlet.2014.05.008>
- E.E. Elemike, D.C. Onwudiwe, D.F. Ogeleka, *J. InorgOrganometPolym.* **29**, 1798–1806 (2019). <https://doi.org/10.1007/s10904-019-01142-y>
- D. Das, R.K. Mohapatra, P.K. Parhi, A.K. Sarangi, R. Sahu, R.S. Barik, *ACS Omega* **5**, 7716–7721 (2020)
- D. Das, A.K. Sarangi, R.K. Mohapatra, P.K. Parhi, A. Mahal, R. Sahu, Md Kudrat-E-Zahan, *J. Mol. Liq.* **309**, 113133 (2020)
- D. Das, S. Pattanaik, P.K. Parhi, R.K. Mohapatra, R.K. Jyothi, L. Jin-Young, H.I. Kim, *ACS Omega* **4**(25), 21604–21611 (2019)
- A. Routray, P.K. Senapati, M. Padhy, D. Das, R.K. Mohapatra, *Int. J. Coal Prep. Util.* (2019). <https://doi.org/10.1080/19392699.2019.1674843>
- M. Sakir, S.M. Onses, *Results Phys.* **12**, 1133–1141 (2019)
- S. Bhakya, S. Muthukrishnan, M. Sukumaran, M. Muthukumar, K.T. Senthul, M.V. Rao, *J. Bioremed. Biodegr.* **6**, 1–9 (2015)
- A. Ucar, M. Findik, I.H. Gubbuk, N. Kocak, H. Bingol, *Mater. Chem. Phys.* **196**, 21–28 (2017)
- S. Kamaljit, A. Sucharita, *Crit. Rev. Environ. Sci. Technol.* **41**(9), 807–878 (2011). <https://doi.org/10.1080/10643380903218376>
- F. Xu, Y. Yuan, D. Wu, M. Zhao, Z. Gao, K. Jiang, *Mater. Res. Bull.* **48**, 2066–2070 (2013)
- E.E. Elemike, D.C. Onwudiwe, L. Wei, L. Chaogang, Z. Zhiwei, *J. Environ. Chem. Eng.* **7**, 103190 (2019)
- X. Chen, Z. Wu, D. Liu, Z. Gao, *Bull. Chem Soc. Ethiop.* **31**, 4–13 (2017)
- T. Mulla, S. Patil, S. Sistla, J. Jadhav, *Biochem. Res. Int.* (2019). <https://doi.org/10.1155/2019/8284968>
- H.S. Abdillahi, J.F. Finnie, J.V. Staden, *J. Ethnopharmacol.* **136**(3), 496–503 (2011)
- P.V. Bruyns, *Bolhalia* **42**(2), 117–245 (2012)
- N.I.F. Morah, W.W. Okoi, *Int. J. Adv. Sci. Res.* **1**(1), 08–09 (2016)
- J. Sharifi-Rad, S.M. Hoseini-Alfatemi, A. Miri, M. Sharifi-Rad, L. Soufi, M. Sharifi-Rad, W.N. Setzer, M. Hoseini, M. Sharifi-Rad, M. Rokni, *Environ. Exp. Biol.* **13**, 169–175 (2015)
- X. Dewanto, K. Wu, K. Adom, R.H. Liu, *J. Agric. Food Chem.* **50**, 3010–3014 (2002)
- R. Yuvakkumar, J. Suresh, A.J. Nathanael, M. Sundrarajan, S.I. Hong, *Mater. Sci. Eng.* **41**, 17–27 (2014)
- E. Varghese, M. George, *Int. J. Adv. Res. Sci. Eng.* **4**(1), 307–314 (2015)
- N. Basavegowda, A. Idhayadhulla, Y.R. Lee, *Mater. Sci. Eng. C* **43**, 58–64 (2014)
- M.L. Curri, R. Comparelli, P.D. Cozzoli, G. Mascolo, A. Agostiano, *Mater. Sci. Eng. C* **23**, 285–289 (2003)
- D. Suresh, R.M. Shobharani, P.C. Nethravathi, M.A.P. Kumar, H. Nagabhushana, S.C. Sharma, *Spectrochim. Acta Part A* **141**, 128–134 (2015)
- R.R. Khoushika, B. Durairaj, *Int. J. App. Pharm.* **9**(5), 116–120 (2017)
- A. Datta, C. Patra, H. Bharadwaj, S. Kaur, N. Dimri, R. Khajuria, *J. Biotechnol. Biomater.* **7**, 271 (2017). <https://doi.org/10.4172/2155-952X.1000271>
- M. Gupta, R.S. Tomar, S. Kaushik, K.R. Mishra, D. Sharma, *Front. Microbiol.* **9**, 2030–2043 (2018). <https://doi.org/10.3389/fmicb.2018.02030>
- I. Fatimah, R.Y. Pradita, A. Nurfalinda, *Int. Conf. Process Eng. Adv. Mater. Proc. Eng.* **148**, 43–48 (2016). <https://doi.org/10.1016/j.proeng.2016.06.483>
- D. Gnanasangeetha, S.D. Thambavani, *Int. J. Pharm. Sci. Res.* **5**(7), 2866–2873 (2014)
- W. Khan, Z.A. Khan, A.A. Saad, S. Shervani, A. Saleem, A.H. Naqvi, *Int. J. Mod. Phys.* **22**, 630–636 (2013)
- M. Romero-Sáez, L. Jaramillo, R. Saravanan, N. Benito, E. Pabón, E. Mosquera, F. Gracia, *Express Polym. Lett.* **11**, 899–909 (2017)
- T. Kokila, P.S. Ramesh, D. Geetha, *Appl. Nanosci.* **5**, 911–920 (2015)
- Z.E.J. Pérez, R. Mathiyalagan, J. Markus, Y.J. Kim, H.M. Kang, R. Abbai, K.H. Seo, D. Wang, V. Soshnikova, D.C. Yang, *Int. J. Nanomed.* **12**, 709 (2017). <https://doi.org/10.2147/IJN.S118373>
- J. Markus, D. Wang, Y.J. Kim, S. Ahn, R. Mathiyalagan, C. Wang, D.C. Yang, *Nanoscale Res. Lett.* **12**, 46 (2017). <https://doi.org/10.1186/s11671-017-1833-2>
- E.J. Rupa, L. Kaliraj, S. Abid, Y. Deok-Chun, J. Seok-Kyu, *Nanomaterials* **9**, 1692 (2019). <https://doi.org/10.3390/nano9121692>
- M.H. Kahsay, A. Tadesse, D. RamaDevi, N. Belachew, K. Basavaiah, *RSC Adv.* **9**, 36967 (2019)
- Z. Tao, X. Yu, J. Liu, L. Yang, S. Yang, *J. Alloys Compd.* **459**, 395–398 (2008)
- T. Islam, A. Dominguez, B. Alvarado-Tenorio, R.A. Bernal, M.O. Montes, J.C. Noveron, *ACS Omega* **4**, 6560–6572 (2019). <https://doi.org/10.1021/acsomega.9b00023>
- Z.H. Diao, M.Y. Li, F.Y. Zeng, L. Song, R.L. Qiu, *J. Hazard. Mater. Mater.* **260**, 585–592 (2013)
- Y. Ma, M. Ni, S. Li, *Nanomaterials* **8**, 428 (2018). <https://doi.org/10.3390/nano8060428>
- Q. Wang, C. Cai, M. Wang, Q. Guo, B. Wang, W. Luo, Y. Wang, C. Zhang, L. Zhou, D. Zhang, Z. Tong, Y. Liu, J. Chen, *Materials* (2018). <https://doi.org/10.3390/ma11061004>
- N. Kaneva, A. Bojinova, K. Papazova, *J. Phys* (2015). <https://doi.org/10.1088/1742-6596/682/1/012022>
- Y. Chiu, T.M. Chang, C. Chen, M. Sone, Y. Hsu, *Catalysts* **9**, 430 (2019). <https://doi.org/10.3390/catal9050430>
- K. Singh, S. Arora, *Crit. Rev. Environ. Sci. Technol.* **41**(9), 807–878 (2011). <https://doi.org/10.1080/10643380903218376>
- M.M. Khan, J. Lee, M.H. Cho, *J. Ind. Eng. Chem.* **20**(4), 1584–1590 (2014)
- S. Senapati, S.K. Srivastava, S.B. Singh, *Nanoscale* **4**(20), 6604–6612 (2012)

50. X. Chen, Z. Wu, D. Liu, Z. Gao, *Nanoscale Res. Lett.* **12**, 143 (2017)
51. K.R. Raajshree, B. Durairaj, *Int. J. Appl. Pharm.* **9**, 20 (2017). <https://doi.org/10.22159/ijap.2017v9i5.20847>
52. L. Yung-Sheng, C. Hui-Ju, H. Jung-Ping, L. Pei-Chi, T. Ching-Ru, H. Tzu-Fang, H. Wen-Ying, *BioMed Res. Int.* (2017). <https://doi.org/10.1155/2017/5232680>
53. Z. Ashraf, M. Rafiq, H. Nadeem, M. Hassan, S. Afzal, M. Waseem, K. Afzal, J. Latip, *PLoS ONE* **12**, 5 (2017). <https://doi.org/10.1371/journal.pone.0178069>

Publisher's Note Springer Nature remains neutral with regard to jurisdictional claims in published maps and institutional affiliations.